

Phase Plane Analysis in Bundle Flow

J. S. Kim^{a*}, Y. Huh^b, and C. Cherif^c

^a Department of Textile Engineering, Graduate School, Kyunghee University, Yongin, 449-701, Korea

^b Faculty of Mechanical and Industrial Systems Engineering, Kyunghee University, Yongin, 449-701, Korea

^c Department of Mechanical Engineering, TU-Dresden, Dresden, 01062, Germany

Abstract

In a roll draft mechanism “draft wave” caused by irregular behavior of floating fibers has been known to occur, which influences directly the thickness variation in the output fiber bundle due to the process resonance in bundle flow. However, in spite of such an important notion of the draft wave, there have scarcely been studies that could explain the existence or the phenomenon since the first conceptual suggestion by W. L. Balls in 1928. In this paper, based on the governing equations (nonlinear PDEs system) for bundle flow, we tried to analyze the dynamic characteristics of the bundle flow in a roll draft system by applying both the linear stability and phase plane analysis, and thus to verify the occurrence of the draft wave. Therefore, the steady state stability and the eigenvalue problem were treated to find the stability diagram, and the solutions of the equations in transient state were obtained by developing a numerical program to illustrate the trajectory of output thickness in a phase plane. Results show that the linear stability can be applied to analyze the bundle flow dynamics. Nonlinearity of the bundle flow reveals that the system oscillates at the critical draw ratio harmonically, indicating the onset of a Hopf bifurcation. For draft ratios above a critical value, the fluctuation in amplitude is amplified, and a sustained oscillation can be achieved. We could confirm that the roller drafting operation has a “bifurcation” property with which the topological structure of phase portrait changes as the draft ratio and the model parameters are varied. When the process variables or model parameters exceed some critical values, fixed points are destroyed and oscillations with the limit cycle occur, which can be called “draft wave”. Particularly, as the value of a draft ratio increases, the phase portrait converges to a shell-shaped curve.

Keywords: Bundle flow; Linear stability; Transient state; Phase plane analysis; Draft wave; Bifurcation

1. Introduction

Roll drafting, an important operation to attenuate the thickness of the bundle and at the same time to get the fibers straightened along the bundle axis, is widely used in staple yarn formation process as an individual process or as a part of a machine unit. However, it is hardly realizable to control the motion of each fiber or fiber groups completely by rollers. Result is the unevenness of the fiber bundle. The fluctuation of the bundle thickness could be more or less minimized in industry by experimental trial and error method based on the engineering sense, though. There have been many researches performed to model the mechanism on the unevenness of fiber bundle theoretically [1-4], or to establish a relationship between the unevenness and the process factors [5-9]. In spite of so much effort to improve the process productivity and textile qualities, the question remains still unsolved how to describe the mechanism of unevenness occurring during a roll drafting theoretically and how to minimize it.

This paper is to analyze the draft dynamics and the unevenness of fiber bundle based on the bundle flow model. By applying the linear stability analysis method the criterion of system stability was established according to various draft ratios and model parameters, namely stability diagram. For a transient flow the solutions of the full nonlinear governing equations were obtained by developing a numerical analysis program and also the phase portraits of them in a phase plane were investigated to various process variables.

2. Governing equations for bundle flow

In a draft system, the fibers nipped by paired rollers restrain the free movement of individual fibers, but in the distance between the nipping positions the fibers flow shearing each other, which cause the number of fibers per cross-section of the flowing bundle to reduce, yielding a thickness attenuation. Figure 1 shows the schematic representation of bundle flow in a drafting process.

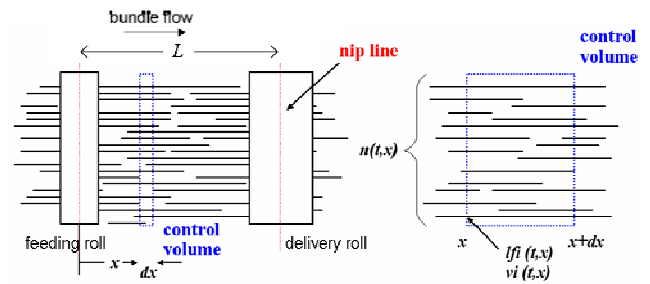


Fig. 1 Schematic drawing of the drafting zone

The model describing the fiber bundle flow in a drafting zone was suggested in our previous study [10]. It consists of a continuity equation, the equation of motion involving velocity variance and a constitutive equation. They are described in terms of the average velocity of the bundle, the linear density, and velocity variance as functions of time and position.

The governing equations are given as follows:

$$(l_b)_t = -(l_b \cdot v)_x \quad (1)$$

$$(l_b \cdot v)_t = -(l_b \cdot v^2)_x - (l_b \cdot \text{Var}[v_i])_x + (f)_x \quad (2)$$

The constitutive equation is assumed as

$$f \propto l_b \cdot (v)_x = \mu \cdot l_b \cdot (v)_x, \quad (3)$$

and the velocity variance of fibers could presumably be taken as

$$\text{Var}[v_i] = a_0 \cdot v \cdot \left(1 - \cos \frac{2\pi}{L} x\right), \quad (4)$$

where l_b , v , t , x , f , $\text{Var}[v_i]$, and L denote the linear density of fiber bundle, the mean velocity of fibers, time, distance in the flow direction, surface force acting on fibers, velocity variance of fibers, and length of flow field (drafting zone), respectively, and subscripts denote partial differentiation. μ and a_0 represent the model parameters that relate to the material properties such as inter-fiber friction, surface characteristics of fiber, fiber length distribution, fiber orientation, etc., and to the process conditions, respectively.

For convenience to work with the equations, we defined dimensionless variables by introducing some scaling factors. Applying the scales

$$x = x^* \cdot L, \quad t = t^* \cdot \frac{L}{v_0}, \quad v = v^* \cdot v_0, \quad l_b = l_b^* \cdot l_{b0} \quad (5)$$

and rearranging the Eqs. (1)~(4) lead to

$$(l_b^*)_t + (l_b^* \cdot v^*)_x = 0 \quad (6)$$

$$(l_b^* \cdot v^*)_t + (l_b^* \cdot v^{*2})_x + a_e \cdot (l_b^* \cdot v^* \cdot (1 - \cos(2\pi x^*)))_x = \mu_e \cdot (l_b^* \cdot (v^*)_x)_x \quad (7)$$

Substituting Eq. (6) into Eq. (7) yields

$$l_b^* \cdot (v^*)_t + l_b^* \cdot v^* \cdot (v^*)_x + a_e \cdot (l_b^* \cdot v^* \cdot (1 - \cos(2\pi x^*)))_x = \mu_e \cdot (l_b^* \cdot (v^*)_x)_x$$

$$\text{where } a_e = \frac{a_0}{v_0}, \quad \mu_e = \frac{\mu}{L \cdot v_0}. \quad (8)$$

The boundary conditions at two end-points are

$$v_0^* = 1, \quad l_{b0}^* = 1 \quad \text{at } x^* = 0 \quad \text{for all } t^* \\ v_L^* = D_R \text{ (draft ratio)} \quad \text{at } x^* = 1 \quad \text{for all } t^* \quad (9)$$

Note that the boundary condition at the output part of linear density $l_b^*(t^*, x^* = 1)$ can not be defined. From now on we will express all the dimensionless variables not using the superscript (*) to avoid complicated equation forms.

3. Solution procedure

3.1 Linear stability analysis

Linear stability analysis is one of the methods to identify the status of a system on stability and to establish the range of the parameters or process conditions to stabilize the system. That is, finding the critical conditions at the onset of instability. The first step for the linear stability analysis is to linearize the governing equations, Eqs. (6) and (7), by introducing the infinitesimal perturbations to state variables around their steady state as follows [11].

$$l_b(t, x) = l_{bs}(x) + \alpha(x) \cdot e^{\lambda t} \quad (10)$$

$$v(t, x) = v_s(x) + \beta(x) \cdot e^{\lambda t} \quad (11)$$

where subscript s indicates the steady state, α and β are the complex perturbation amplitudes of state variable, and λ is a complex eigenvalue that accounts for the growth rate of the perturbation, where $\text{Re}(\lambda)$ is the growth or decay rate, and $\text{Im}(\lambda)$ the disturbance frequency. The equations in the steady-state flow

are determined from Eqs. (6) and (7) with $\partial(\cdot)/\partial t=0$ [10]. Substitution of Eqs. (10) and (11) into the governing equations, then, leads to the following linearized governing equations:

$$\lambda \cdot \alpha = -v'_s \cdot \alpha - v_s \cdot \alpha' - l'_{bs} \cdot \beta - l_{bs} \cdot \beta' \quad (12)$$

$$= -v'_s \cdot \alpha - v_s \cdot \alpha' + \frac{v'_s}{v_s} \cdot \beta - \frac{1}{v_s} \cdot \beta'$$

$$\lambda \cdot \beta = -\{a_e \cdot (1 - \cos(2\pi x)) \cdot v_s \cdot v'_s + 2\pi \cdot a_e \cdot \sin(2\pi x) \cdot v_s^2 \\ - \mu_e \cdot v_s \cdot v_s'' + v_s^2 \cdot v_s'\} \cdot \alpha \quad (13)$$

$$- \{a_e \cdot (1 - \cos(2\pi x)) \cdot v_s^2 - \mu_e \cdot v_s \cdot v_s'\} \cdot \alpha'$$

$$- \left\{ 2\pi \cdot a_e \cdot \sin(2\pi x) - a_e \cdot (1 - \cos(2\pi x)) \cdot \frac{v'_s}{v_s} + v'_s \right\} \cdot \beta$$

$$- \left\{ a_e \cdot (1 - \cos(2\pi x)) + \mu_e \cdot \frac{v'_s}{v_s} + v_s \right\} \cdot \beta' + \{ \mu_e \} \cdot \beta''$$

$$\text{Boundary conditions: } \alpha(0) = \beta(0) = \beta(1) = 0. \quad (14)$$

Here, superscript (') denotes derivative of state variables with respect to distance from inlet, x . The above equations with boundary conditions constitute an eigenvalue problem. Therefore, to evaluate eigenmodes of the linearized equations given above, we set up an eigenmatrix system by discretizing Eqs. (12) and (13), using a proper finite difference scheme and rearranging them:

$$\lambda I \bar{\gamma} = A \bar{\gamma} \quad \text{or} \quad (A - \lambda I) \bar{\gamma} = \bar{0} \quad (15)$$

where $\bar{\gamma} = [\alpha_1, \alpha_2, \dots, \alpha_n, \beta_1, \beta_2, \dots, \beta_{n-1}]^T$ and A is matrix whose components are obtained from the algebraic manipulations of Eqs. (12) and (13). The stability of system is then determined by eigenvalues, λ . If the real part of any eigenvalue of λ for a given condition is found positive, then the system is unstable indicating an unbounded growth of state variables with time.

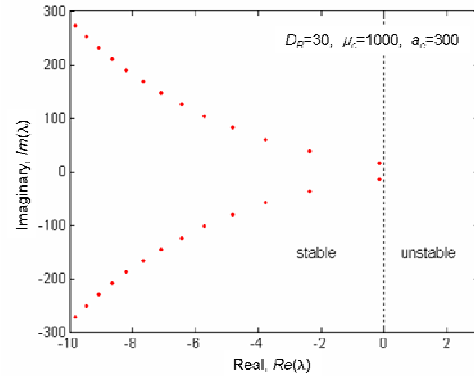


Fig. 2 Eigenvalue spectra for $D_R=30$, $\mu_e=1000$, and $a_e=300$.

Figure 2 shows, for instance, a typical result of the eigenvalue problem for the given values of $D_R=30$, $\mu_e=1000$, and $a_e=300$. In this case, since all the eigenvalues are laid on the left half-plane, this flow is stable. If at least one eigenvalue crosses into the right half-plane, the flow becomes unstable.

Representing the real parts of the largest eigenvalues ($\text{Re}(\lambda)_{\max}$) according to various draft ratios is given in Figure 3. For constant μ_e and a_e , there exists only one crossing point where the sign of the $\text{Re}(\lambda)_{\max}$ changes against D_R . We also can observe a crossing point in a higher draft ratio as the dimensionless parameter a_e increases. Figure 4 shows the profile of $\text{Re}(\lambda)_{\max}$ with respect to μ_e under the constant values of D_R and a_e . As μ_e increases, the profile of $\text{Re}(\lambda)_{\max}$ intersects with zero value two

times at point A and A' for $D_R=30$, whereas it takes zero at only one point A'' for $D_R=10$. This means that the transition from a stable state to an unstable one depends on the relationship of D_R with the dimensionless parameters.

In this study, however, we don't consider the bundle flow at the point A' and A''. (The reason is going to be explained in section 4.1.)

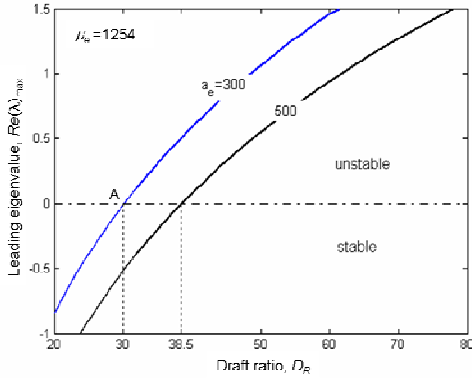


Fig. 3 Real part of leading eigenvalue with respect to draft ratio in different dimensionless parameter a_e .

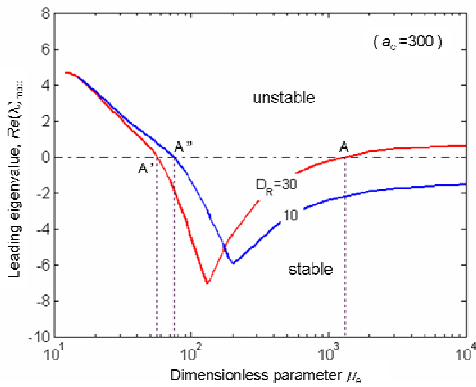


Fig. 4 Real part of leading eigenvalue against dimensionless parameter μ_e with the change of draft ratio

3.2 Solution of the nonlinear problem

Transient solutions of the nonlinear governing Eqs. (6) and (7) have been obtained using a FTCS (Forward Time and Backward space) differencing based on the Explicit-Implicit hybrid scheme to avoid the numerical instability problems due to the model parameters. The grid sized for x and t are selected as $\Delta x=2 \times 10^{-2}$ and $\Delta t=1 \times 10^{-4}$, respectively, considering the accuracy for numerical solutions. The simulation program was developed using software MATLAB®. The produced plots could be saved, printed or exported in Windows Bitmap format, while the calculated values be viewed and saved.

4. Results and discussion

4.1 Steady state flow

The bundle flow in a steady state was investigated by varying the dimensionless parameter $\mu_e=60, 100$, and 300 for the draft ratio $D_R=30$, and the parameter $a_e=300$. The flow response is depicted in Figure 5, where the distributions of the velocity, $v_s(x)$, and the bundle thickness, $l_{bs}(x)$, in a drafting zone are plotted against the position x . From figure 5a), the velocity increases

monotonically with the position x for a given value of $\mu_e=300$, while the curvature of the profile becomes stronger as the value of μ_e decreases. In particular, for $\mu_e=60$, the flow shows a noticeable behavior that the velocity of bundle is faster than that of front roller near the exit.

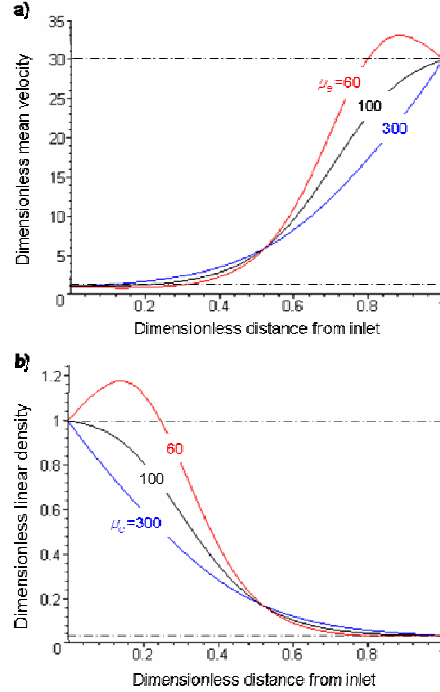


Fig. 5 Distributions of a) dimensionless velocity and b) linear density of fiber bundle in a steady state flow. ($D_R=30, a_e=300, \mu_e=60, 100, 300$)

The linear density profiles (Fig. 5b) show the reciprocal relation to the velocity profiles under the steady state condition. For $\mu_e=60$, especially, the linear density distribution exhibits an overflow-like behavior near the inlet. Since the velocity (the linear density) distribution, however, should be limited within the range of between 1 and D_R (the range of $[1, 1/D_R]$) for an extensional bundle flow such as drafting process, the flow type shown under the condition of $\mu_e=60, a_e=300$, and $D_R=30$ can not be expected in a practical process.

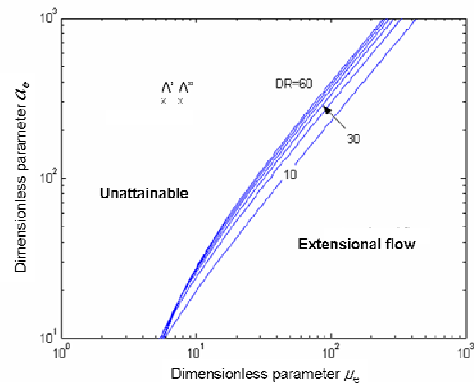


Fig. 6 Unattainable region of the dimensionless parameters to several draft ratios in an extensional bundle flow.

Figure 6 shows an unattainable region of the dimensionless parameters in an extensional bundle flow. It is shown that the

extensional bundle flow can take place in a specific region of the parameters for a given D_R (the right hand side of curve). For given values of D_R and μ_e the parameter value of a_e is ceiled. Note that the A' and A'' pointed out on figure 4 is placed within the unattainable region.

4.2 Bifurcations on linear stability

To establish the criterion for the stability of bundle flow to the draft ratio and the dimensionless parameters we estimated the critical values in which $Re(\lambda)_{max}$ becomes zero, and thus obtained a stability diagram as shown in Figure 7. In these figures, solid lines denote the critical values which divide the parameter domain into stable and unstable zones. Dotted lines stand for the boundary between the zone where extension bundle flow occurs and the unattainable region. Figure 7a) depicts the critical draft ratios $(D_R)_c$ to the dimensionless parameters. Independently of the value of a_e , the system can be unstable for a large value of μ_e , when the draft ratio becomes larger than 20.93. As the dimensionless parameter a_e decreases, the stable chimney region is located at lower values of μ_e .

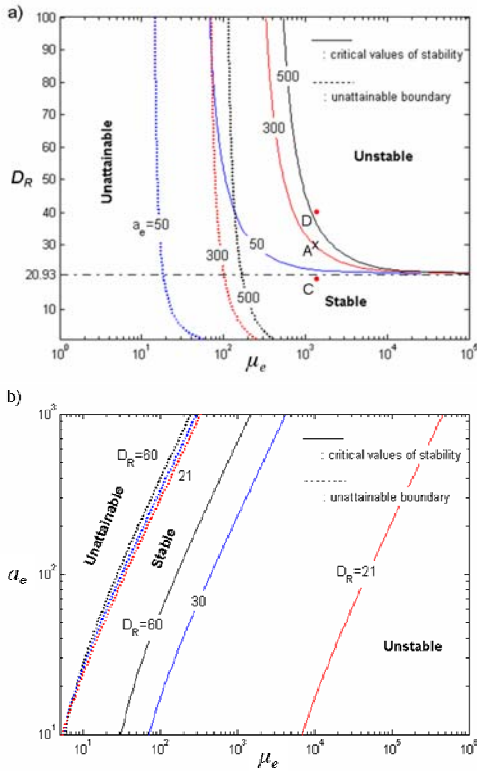


Fig. 7 Stability diagram for bundle flow: a) critical draft ratio to the dimensionless parameters, b) the relationship between dimensionless parameters μ_e and a_e to the draft ratio

Figure 7b) represents the stability diagram in parameter space. The parameter plane can be divided into 3 zones, that is, unattainable zone, stable zone, and the unstable zone. The stable zone is placed between the unattainable zone and the unstable. In addition, the stable zone becomes narrow as the draft ratio increases, while below $D_R=20.93$, the flow is always stable, independent of the parameters μ_e and a_e . In other words, the transition from stable behavior to unstable one occurs as D_R and μ_e increase and a_e decreases. Therefore, we can recognize that the bundle flow undergoes a supercritical Hopf bifurcation for D_R

and μ_e , while it has characteristics of subcritical Hopf bifurcation for a_e .

4.3 Transient response of the bundle thickness

Based on the linear stability results and on the numerical solutions of the nonlinear governing equations, the nonlinear dynamics of the bundle flow was analyzed.

4.3.1 Unsteady flow

Figure 8 is a simulation result in a 3-dimensional picture of the bundle thickness in a flow field, clearly showing the fluctuations with respect to time. The simulation condition of $D_R=40$, $\mu_e=1,254$, $a_e=300$ corresponds to the point D indicated in Figure 7a), which is located in the unstable zone for the linearized system.

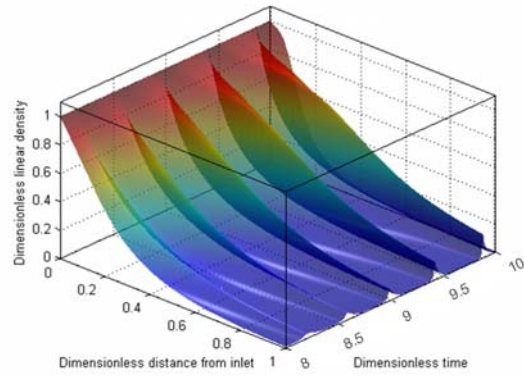


Fig. 8 Tree-dimensional transient picture of the bundle thickness in a flow field: $D_R=40$, $\mu_e=1,254$, $a_e=300$.

But the simulation applied to the nonlinear bundle flow system shows that the thickness profile fluctuates with a constant amplitude and a period T . This is illustrated in Figure 9, where the bundle thickness is plotted against the position x at $t=0$, $T/5$, $2T/5$, $3T/5$, and $4T/5$.

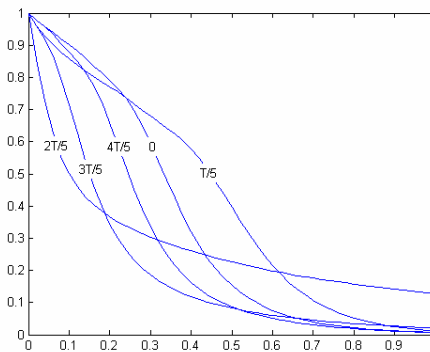


Fig. 9 Linear density distributions of fiber bundle in a drafting zone with time elapse during one oscillation period: $D_R=40$, $\mu_e=1,254$, $a_e=300$

The spatial response of bundle thickness under transient condition, namely the dependence of the oscillatory behavior on position is depicted in Figure 10, showing the temporal thickness behavior at different positions $x=1/8$, $1/4$, $1/2$, $3/4$, and 1 . It is shown that the whole system oscillates at the same frequency with different phase (the phase is dependent on the bundle velocity at a position x). The shape of the waveform near the inlet

($x=1/8$) exhibits an oscillation with broad bell-shaped peaks and narrow bottoms. At the midpoint, however, the shape is reversed. As the bundle approaches to output position, the picks become narrower and the bottoms become wider.

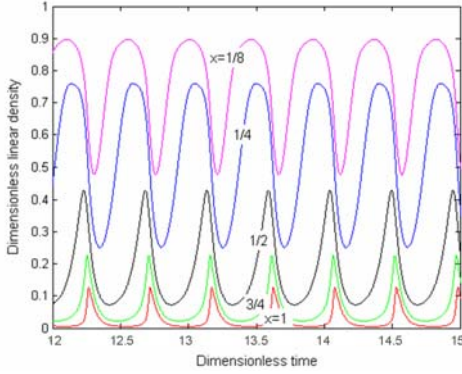


Fig. 10 Temporal pictures at different positions within drafting zone: $D_R=40$, $\mu_e=1,254$, $a_e=300$

4.3.2 Phase plane analysis

To investigate the effect of draft ratio on the dynamic characteristics of bundle flow, the transient behavior of output linear density is simulated for three draft ratios: $D_R=20$, 30, and 40, corresponding to C, A, and D in Figure 7a), while the dimensionless parameters μ_e and a_e are set equal to 1,254 and 300, respectively (Fig. 11). Figure 11a) shows that, for the draft ratio of 20, the output bundle thickness exhibits a damped oscillatory behavior. The fluctuations decay with time after “ringing” symmetrically with respect to a fixed point for a while, and then, the steady state is attained. If the decay becomes slower and finally reaches at a critical draft ratio $(D_R)_c$, the equilibrium state can lose its stability as shown in Fig 11b). As the draft ratio D_R increases further, the sustained oscillation in output bundle thickness changes into the oscillation with increasing amplitude. Figure 11c) shows the increasing magnitude of fluctuation. However, the rate of fluctuation growth diminishes after some time and another sustained oscillation is then achieved. It is noted that beyond the critical draft ratio, the oscillations show asymmetric shape, having narrow and sharp peaks with wide and flat bottoms.

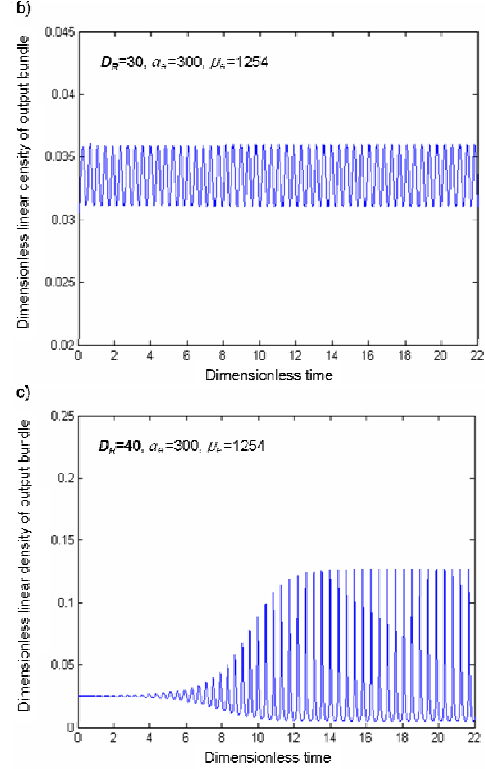
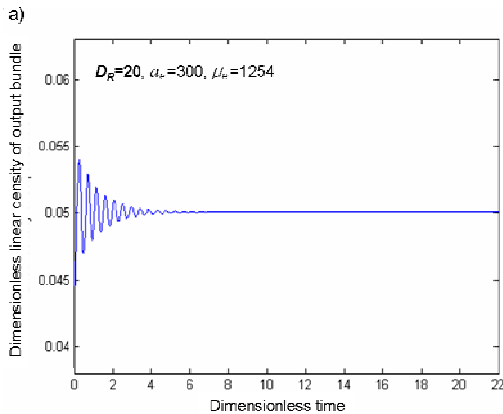
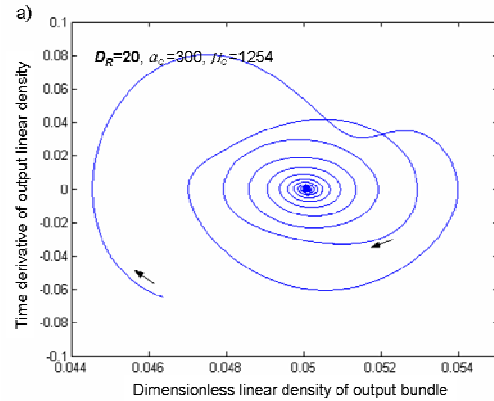


Fig. 11 Temporal pictures of the linear density of output bundle to various draft ratios when $\mu_e=1,254$, and $a_e=300$: a) $D_R=20$, b) $D_R=(D_R)_c=30$, and c) $D_R=40$.

The analysis results hitherto show that the bundle flow has the dynamic characteristics that the draft ratio above a critical value does not allow a fixed point to appear but a limit cycle oscillation which can be defined as “draft wave” and may derive a process resonance.

Dynamics of bundle flow can be described in a more detailed way by the trajectories of the state variables. The output linear density and the linear density change rate were taken as state variables. Trajectories in the phase plane are given in Figure 12. Figure 12a) shows the trajectory that winds down to a stable spiral toward a fixed point for $D_R=20 < (D_R)_c$. For $D_R \geq (D_R)_c$, a cyclic pattern appears. The oscillation is purely harmonic (elliptic limit cycle) and symmetric (Fig. 12b). When $D_R=40$, the trajectory converges to a shell-shaped curve (Fig. 12c). Therefore, we can confirm that the roller drafting operation undergoes a dynamic change of the output bundle thickness, as D_R changes.



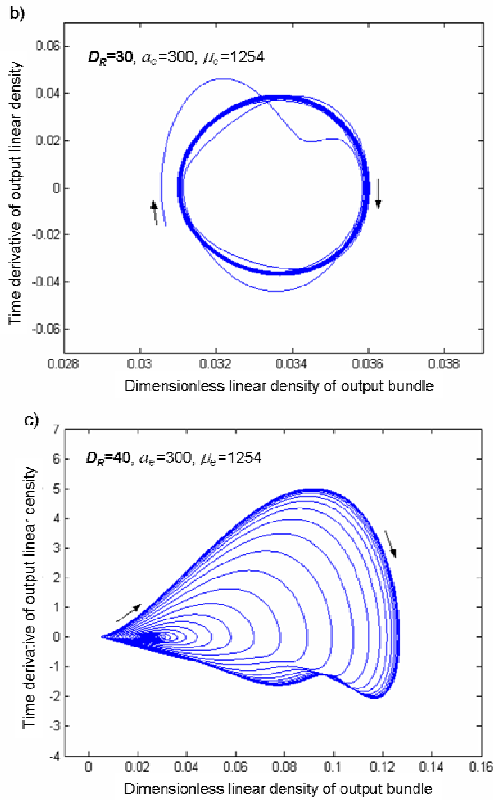


Fig. 12 Trajectories of the linear density of output bundle to various draft ratios when $\mu_e=1254$, and $a_e=300$: a) $D_R=20$, b) $D_R=(D_R)_c=30$, and c) $D_R=40$.

Especially, when the draft ratio is further increased ($D_R=60$), the amplitude of oscillation grows rapidly and the flux reaches more quickly the sustained oscillation (Fig. 13). The wave peaks also become much narrower and sharper with the wave bottoms becoming flatter. But the bundle thickness can reach practically near zero, which means that the bundle rupture can occur around $D_R=60$.

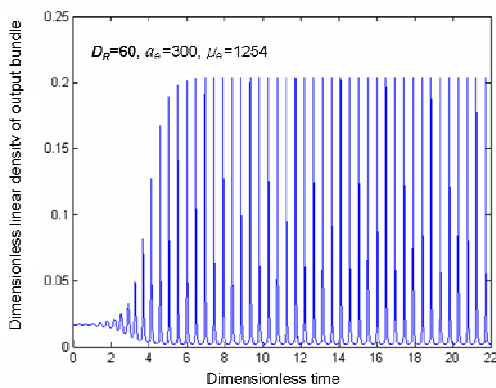


Fig. 13 Temporal pictures of the linear density of output bundle when $D_R=60$, $\mu_e=1254$, and $a_e=300$

5. Conclusion

In this research we tried to analyze the draft dynamics and the nonlinear characteristics of a bundle flow system based on the theoretical model. Linear stability analysis was applied to predict

the critical threshold of system instability, and phase plane analysis was conducted based on the numerical solutions for the nonlinear transient response. For the linear stability analysis, the eigenvalue problem of the linearized bundle flow model was treated. The solution of the nonlinear governing equations system was obtained by a numerical analysis program developed with the application of FTCS method based on the Explicit-Implicit hybrid scheme. The results showed that the linear stability analysis agrees excellently with those by nonlinear transient simulation. A critical draft ratio could be verified not only by the linear stability analysis but also by the transient state analysis. Transition from the stable behavior to the unstable occurs as draft ratio and inter-fiber friction parameter increase and the parameter for the variance of individual fiber speeds decreases. When the draft ratio exceeds the critical value, the fixed point is destroyed and the limit cycle oscillation appears, which leads to the so called "draft wave". For a draft ratio above the specific value, the fluctuations increase but arrive at another level of sustained oscillation.

This study shows an intriguing result about the existence of a specific draft ratio above which the flow can always be unstable, which suggests us a further study on this topic.

Acknowledgements

This work was supported by the Korea Research Foundation Grant funded by the Korean Government (MOEHRD) (KRF-2005-D00931).

References

- [1] P. A. Grishin, Theory of Drafting and Its Practical Applications. J.T.I., 45, 167 (1954).
- [2] J. S. Rao, A Mathematical Model to the Ideal Sliver and Its Application to the Theory of Roller Drafting. J.T.I., 52, 571 (1961).
- [3] H. R. Plonsker and S. Backer, The Dynamics of Roller Drafting. T.R.J., 37, 637 (1967).
- [4] J. S. Rao, Theory of Roller Drafting. J.T.I., 53, T465 (1962).
- [5] H. Balasubramanian, P. Grosberg, and Y. Turkes, Studies in Modern Yarn Production. Textile Institute, Manchester, p150 (1968).
- [6] B. Dutta and P. Grosberg, The Dynamic Response of Drafting Tension to Sinusoidal Variations in Draft Ratio under Conditions of Sliver Elasticity in Short-staple Drafting. J.T.I., 64, 534, (1973).
- [7] G. Mandl and H. Noebauer, The Influence of Cotton-Spinning Machinery on the Random Irregularity of Sliver and Yarns - Part I, II, III. J.T.I., 68, 387, 394, 400, (1977).
- [8] N. A. G. Johnson, A Computer Simulation of Drafting. J.T.I., 72, 69, (1981).
- [9] P. R. Lord and M. Govindaraj, Dynamic Measurement of Mechanical Errors in Sliver-drawing. J.T.I., 81, 195, (1990).
- [10] You Huh and Jong S. Kim, Modeling the Dynamic Behavior of the Fiber Bundle in a Roll-Drafting Process. T.R.J., 74(10), 872, (2004).
- [11] P. G. Darzin, Introduction to Hydrodynamic Stability. Cambridge, (2002).
- [12] Steven H. Strogatz, Nonlinear Dynamics and Chaos. Westview, (2000).